



Cite this: *RSC Adv.*, 2023, **13**, 17968

Semiconductor and topological phases in lateral heterostructures constructed from germanene and AsSb monolayers†

Chu Viet Ha,^a Bich Ngoc Nguyen Thi,^b Pham Quynh Trang,^a R. Ponce-Pérez,^c Vu Thi Kim Lien,^{de} J. Guerrero-Sánchez^c and D. M. Hoat^{*de}

Two-dimensional (2D) heterostructures have attracted a lot of attention due to their novel properties induced by the synergistic effects of the constituent building blocks. In this work, new lateral heterostructures (LHSs) formed by stitching germanene and AsSb monolayers are investigated. First-principles calculations assert the semimetal and semiconductor characters of 2D germanene and AsSb, respectively. The non-magnetic nature is preserved by forming LHSs along the armchair direction, where the band gap of the germanene monolayer can be increased to 0.87 eV. Meanwhile, magnetism may emerge in the zigzag-interline LHSs depending on the chemical composition. Such that, total magnetic moments up to $0.49 \mu_B$ can be obtained, being produced mainly at the interfaces. The calculated band structures show either topological gap or gapless protected interface states, with quantum spin-valley Hall effects and Weyl semimetal characters. The results introduce new lateral heterostructures with novel electronic and magnetic properties, which can be controlled by the interline formation.

Received 22nd March 2023

Accepted 23rd May 2023

DOI: 10.1039/d3ra01867a

rsc.li/rsc-advances

I. Introduction

Stimulated by the successful investigations and applications of graphene and its derivatives,^{1–4} a large variety of two-dimensional (2D) materials have been prepared in experiments and predicted by theoretical calculations.^{5–10} In comparison with their three-dimensional (3D) bulk counterparts, 2D materials usually exhibit unique properties that make them suitable for diverse applications.^{11–14} In addition, different feature-rich characteristics can be obtained by means of surface modification,^{15,16} doping,^{17,18} application of external strain and electric field,^{19–21} and formation of heterostructures. Between them, 2D van der Waals vertical heterostructures (VHSs) – two vertically stacked 2D materials – have been commonly investigated, including ones formed by graphene, boron nitride, and transition metal dichalcogenides (TMDs).^{22–25} Such VHSs exhibit good electrical and optical properties and may be promising candidates for the next generation of optoelectronic

and electronic devices.^{26,27} Besides the development of sophisticated experimental methods and equipment, other fascinating heterostructures, namely lateral heterostructures (LHSs) – where two 2D materials are in-plane interline-connected – have also been synthesized.^{28–31} In these cases, the chemical bonds are formed between constituent edges to create highly stable materials. Lateral heterostructures provide an effective solution for contamination and the difficulty of stacking orientation, that their VHS counterparts suffer, along with the feasibility of planner device integration.³² Until now, research around LHSs has received much less attention than VHSs, and this lack of knowledge on LHSs should be resolved in order to design more 2D materials for practical applications.

The growth of the germanene-2D form of germanium, on either metallic substrates as Au(111),³³ Cu(111),³⁴ Ag(111),³⁵ Pt(111),³⁶ and Al(111),³⁷ or non-metallic substrates as semiconductor MoS₂ (ref. 38) and semimetal Sb(111) has been reported. A germanene monolayer exhibits semimetallic nature with a graphene-like Dirac point, possessing high charge carrier mobility. Therefore, it has been considered as a potential Dirac fermion material to be applied in field-effect transistors with high speed and low energy consumption.^{39,40} In addition, researchers have studied efficient methods to open the germanene monolayer band gap. For example, the semiconductor character with variable energy gap between 0.02 to 0.31 eV can be obtained by adsorption of alkali metals,⁴¹ while a halogenation approach may induce larger values ranging from 0.416 to 1.596 eV depending on the functionalization configuration.⁴²

^aFaculty of Physics, TNU-University of Education, Thai Nguyen, Vietnam

^bInstitute of Physics, Vietnam Academy of Science and Technology, 18 Hoang Quoc Viet, Cau Giay, Hanoi, Vietnam

^cUniversidad Nacional Autónoma de México, Centro de Nanociencias y Nanotecnología, Apartado Postal 14, Ensenada, Baja California, Código Postal 22800, Mexico

^dInstitute of Theoretical and Applied Research, Duy Tan University, Hanoi 100000, Vietnam. E-mail: dominhhoat@duytan.edu.vn

^eFaculty of Natural Sciences, Duy Tan University, Da Nang 550000, Vietnam

† Electronic supplementary information (ESI) available. See DOI: <https://doi.org/10.1039/d3ra01867a>



On the other hand, stimulated by the successful fabrication of phosphorene,^{43,44} researchers have paid special attention to 2D materials based on VA-group atoms including nitrogen,^{45,46} phosphorene,^{47,48} arsenene,^{49,50} antimonene,^{51,52} and bismuthene.^{53,54} Interestingly, they exhibit appropriate electronic band gaps for electronic and optoelectronic applications, presenting an advantage in comparison with those based on IVA-group atoms. It has been found that the chemical combination of VA atoms leads to the fine-tuning of electronic properties to broaden their applications.^{55,56} In this regard, semiconducting 2D VA-VA haeckelite compounds have been predicted by Lin *et al.*,⁵⁷ which crystallize in a buckled tetragonal structure. Results indicate good dynamical stability and moderate band gaps ranging from 0.80 to 2.68 eV of these 2D compounds. Similarly, Yu *et al.*⁵⁸ have investigated the stability and electronic properties of atomically thin binary V-V semiconductor compounds using first-principles calculations. Crystallizing in the α phase (black phosphorene) and β phase (blue phosphorene), these 2D materials exhibit moderate direct and indirect gaps, respectively. Among them, the AsSb monolayer has energy gaps of 0.48 and 1.27 eV, respectively.

In this study, our main aim is to examine the structural, electronic, and magnetic properties of LHSs formed from germanene and AsSb monolayers using density functional theory (DFT) calculations. In total, 14 LHSs with both armchair and zigzag interlines are considered. It is anticipated that the semiconductor nature is obtained by the armchair interlines, which may be a good choice to increase the germanene band gap. Interestingly, despite the non magnetic nature of both building blocks, the zigzag-connection leads to the emergence of a topological phase with significant magnetic properties. Results suggest that the LHS formation may induce novel properties that are not found in the separate constituent monolayers.

II. Computational details

First-principles calculations based on density functional theory (DFT)⁵⁹ are performed in the Vienna *ab initio* Simulation Package (VASP).^{60,61} The projector augmented wave (PAW) and generalized gradient approximation in the Perdew–Burke–Ernzerhof (GGA-PBE) version⁶² are adopted in the calculations. Usually, standard GGA functionals underestimate a materials electronic band gap, this defect can be solved with some advanced approaches such as the hybrid HSE functional.^{63,64} However, HSE-based calculations require high computational cost, specially for large systems containing a large number of atoms. Therefore, we have employed the HSE06 functional only for the AsSb monolayer, meanwhile PBE-based calculations are performed for the LHSs since the PBE functional is proven to describe the electronic profile and magnetic properties of materials well. The plane-wave cutoff kinetic-energy is set to 500 eV, and the first Brillouin zone is integrated using a k -grid size of $2 \times 12 \times 1$, which is generated withing the framework of the Monkhorst–Pack method.⁶⁵ A vacuum gap of 14 Å is set to minimize the periodic interactions between adjacent images. Structural optimization of all considered LHSs is realized by relaxing the constituent atoms until the forces are less than

0.01 eV Å⁻¹. In all calculations, self-consistent calculations are iterated until reaching the energy convergence of 10⁻⁶ eV.

III. Results and discussion

A. Germanene and AsSb monolayers

Germanene monolayers adopt a buckled hexagonal honeycomb structure, belonging to the $P\bar{3}m1$ (no. 164) space group. There are two equivalent germanium (Ge) atoms in a unit cell as displayed in Fig. 1a. The structure of germanene is optimized by relaxing freely atomic positions and unit cell geometry. Our calculations yield the following optimal parameters: (1) lattice constant $a = 4.06$ Å; (2) chemical bond length $d_{\text{Ge-Ge}} = 2.44$ Å; (3) buckling height $\Delta_{\text{Ge-Ge}} = 0.69$; and (4) interatomic angle $\angle = 112.34^\circ$, which are in good agreement with previous calculations.⁶⁶ Fig. 2a shows the calculated electronic band

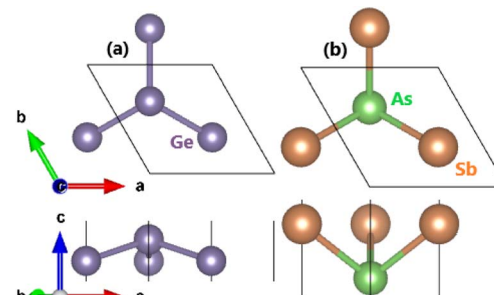


Fig. 1 Atomic structure (unit cell is marked) of (a) germanene and (b) AsSb monolayer.

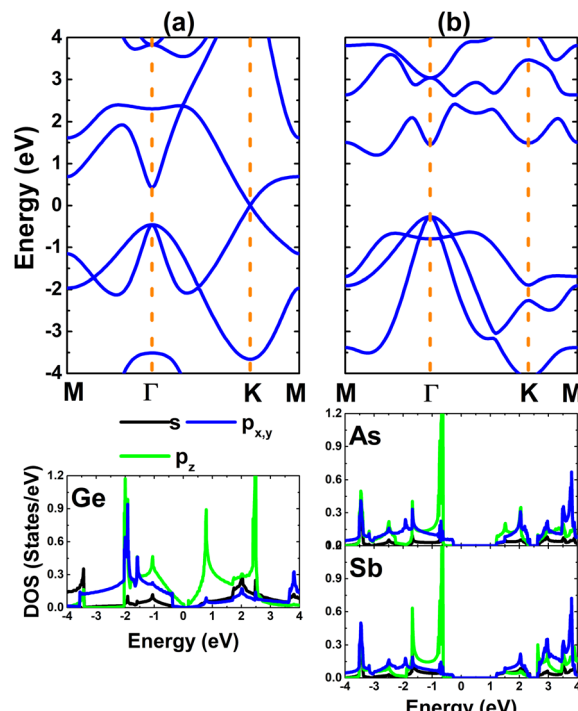


Fig. 2 Electronic band structure and projected density of states of (a) germanene and (b) AsSb monolayer.

structure and projected density of states (PDOS) of the germanene monolayer. The semimetallic character can be noted with a Dirac cone at the K point. In the considered energy from -4 to 4 eV, the band structure is formed from both the s orbital (s state) and p orbital ($p_{x,y}$ and p_z states). As a characteristic of hexagonal 2D materials, p_x and p_y are degenerate,^{67,68} and are submerged in both the valence band and conduction band of the germanene monolayer. Meanwhile, the p_z state is the main contributor at the vicinity of the Fermi level to the Dirac cone.

A similar structure is considered for the AsSb monolayer (β phase) by alternating the arsenic (As) and antimony (Sb) atoms in a unit cell (see Fig. 1b). The following structural parameters can describe the optimized unit cell: (1) lattice constant $a = 3.86$ Å; (2) chemical bond length $d_{\text{As-Sb}} = 2.70$ Å; (3) wrinkle $\Delta_{\text{As-Sb}} = 1.52$ Å; and (4) interatomic angle $\angle \text{AsSbAs} = \angle \text{SbAsSb} = 91.47^\circ$. To examine the stability of this monolayer, the phonon dispersion curves are calculated. The results are displayed in

Fig. 3. Considering two atoms ($N = 2$) in a primitive cell, the phonon spectra are composed of $3N = 6$ phonon modes (between them 3 acoustic modes and $3N - 3 = 3$ optical modes). Most importantly, there is no imaginary phonon frequency to confirm that the AsSb monolayer is dynamically stable. The band structure and PDOS spectra are given in Fig. 2b. The AsSb monolayer is an indirect gap semiconductor considering the valence band maximum (VBM) and conduction band minimum (CBM) located at the Γ point and along the $M\Gamma$ direction, respectively. The obtained indirect gap value is 1.47 eV, which agrees well with previous calculations.⁵⁸ In addition, HSE06-based calculations provide a larger band gap of 2.05 eV (see Fig. S1 of the ESI†). In the considered energy range, both constituents form the band structure: due to their similar valence electronic configurations, the As($4s^24p^3$) and Sb($5s^25p^3$) atoms exhibit similar PDOS spectra, where the band gap originates from the separation of electronic states belonging to the p orbitals.

Next, the formation of lateral heterostructures was studied. The lattice mismatch m is calculated as follows:¹⁰

$$m = \frac{2 \times |a_{\text{germanene}} - a_{\text{AsSb}}|}{a_{\text{germanene}} + a_{\text{AsSb}}} \times 100\% \quad (1)$$

A small lattice mismatch of 5.05% is obtained, suggesting the feasibility of constructing lateral heterostructures from germanene and AsSb monolayers. In this work, a new set of $(\text{Ge})_m-(\text{AsSb})_{8-m}$ with both armchair (A-) and zigzag (Z-) interlines are investigated. Fig. 4 shows the atomic structure of A-(Ge)₄-(AsSb)₄ and Z-(Ge)₄-(AsSb)₄ LHSs with 32 atoms in a unit cell, where the initial building blocks are clearly indicated. The formation energy E_f is calculated using the following expression:⁶⁹

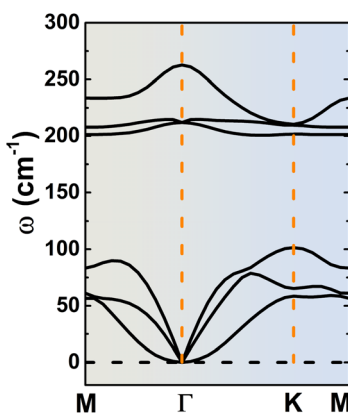


Fig. 3 Phonon dispersion curves of the AsSb monolayer.

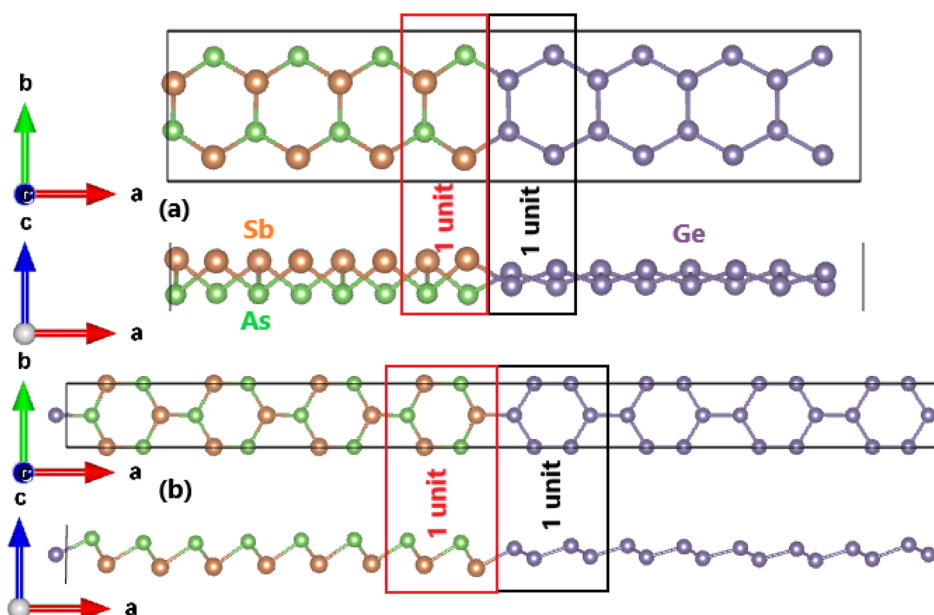


Fig. 4 Atomic structure of (a) armchair- and (b) zigzag-interline $(\text{Ge})_4-(\text{AsSb})_4$ lateral heterostructures.



$$E_f = E_{\text{LHS}} - 2mE_{\text{germanene}} - 2(8 - m)E_{\text{AsSb}} \quad (2)$$

where the total energies of the LHS, germanene, and AsSb monolayer are denoted by E_{LHS} , $E_{\text{germanene}}$, and E_{AsSb} , respectively. The results are given in Fig. 5. A slight variation of E_f with chemical composition is found. Moreover, the formation of A-LHSs (with E_f between 0.44 and 0.54 eV) require higher energy than Z-LHSs (between 0.32 and 0.44 eV). In order to analyze the thermal stability of $(\text{Ge})_m-(\text{AsSb})_{8-m}$ LHSs, *Ab Initio* Molecular Dynamics (AIMD) simulations are carried out. The results indicate that all studied LHSs are thermally stable at 300 K considering the absence of structural destruction over a large time range of up to 3000 fs (see Fig. S2 of the ESI[†]). It is suggested to prepare these LHSs by means of chemical vapor deposition⁷⁰ or molecular beam epitaxy,⁷¹ methods which have been widely used to grow a large variety of 2D materials of large size and high quality. So far, experimental investigations have reported the preferable formation of a zigzag interface, meanwhile the armchair interline is only occasionally seen.^{29,72} Therefore, germanene–AsSb Z-LHSs are expected to be formed more easily than their A-counterpart, which is in agreement with the calculated formation energies.

B. Armchair-interline lateral heterostructures

As a first step, the LHSs structures are optimized by freely relaxing the constituent atoms and unit cell geometry. Fig. 6 shows the calculated lattice constants. Remembering that germanene has a larger lattice constant than the AsSb monolayer, consequently, the LHSs unit cell dimensions increase nearly linearly with the number of germanene units. Moreover, there is an abrupt variation of the buckling height at the interface due to each side preserving its original wrinkle (see Fig. 4a).

The calculated band structures are displayed in Fig. 7, which show the semiconductor nature of the armchair-interline lateral heterostructures. The direct gap character of $(\text{Ge})_5-(\text{AsSb})_3$ and $(\text{Ge})_7-(\text{AsSb})_1$ LHSs can be noted, considering the location of both the VBM and CBM at the X point, meanwhile the remaining LHSs are indirect gap semiconductors since their VBM and CBM take place at different high symmetry points. Therefore, the indirect-to-direct gap transition may occur by simply varying the number of building blocks in the lateral

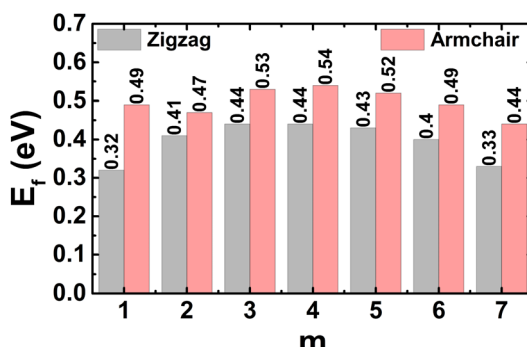


Fig. 5 Formation energy of $(\text{Ge})_m-(\text{AsSb})_{8-m}$ lateral heterostructures with armchair- and zigzag-interline.

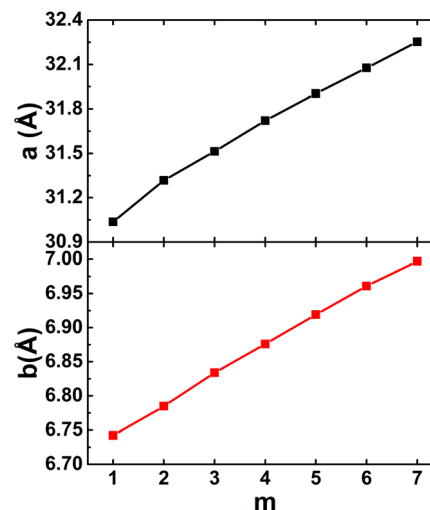


Fig. 6 Lattice constants of armchair-interline $(\text{Ge})_m-(\text{AsSb})_{8-m}$ lateral heterostructures.

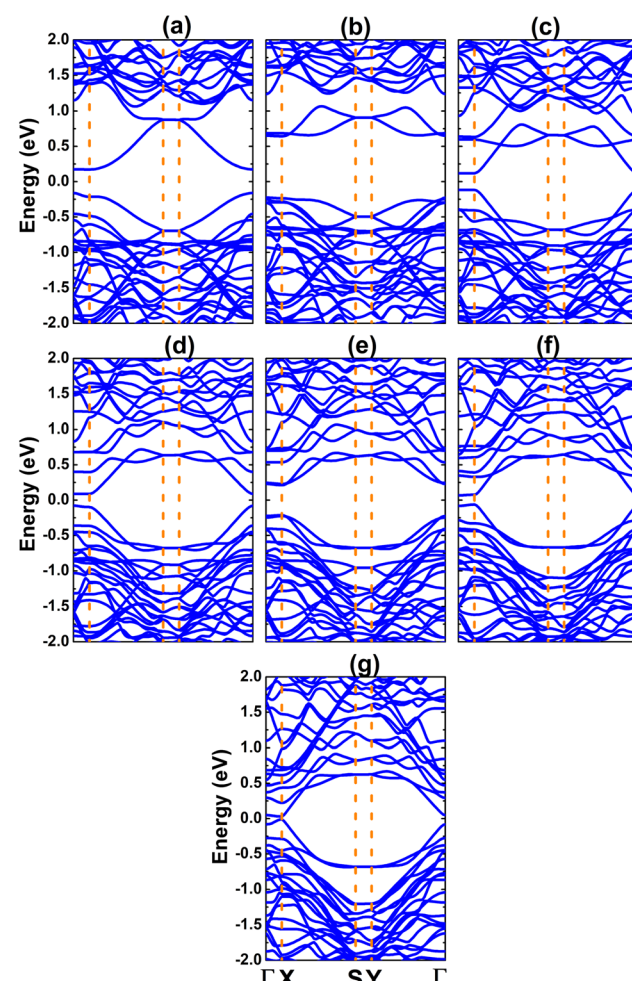


Fig. 7 Electronic band structure (blue curves: non-spin-polarization) of armchair-interline $(\text{Ge})_m-(\text{AsSb})_{8-m}$ lateral heterostructures with (a) $m = 1$, (b) $m = 2$, (c) $m = 3$, (d) $m = 4$, (e) $m = 5$, (f) $m = 6$, and (g) $m = 7$.



heterostructure. The calculated energy gaps are given in Fig. 8. Note that this parameter depends strongly on the chemical composition. The largest band gap of 0.87 eV is obtained with 25% germanene ($m = 2$). Meanwhile, a large germanene composition of 87.5% ($m = 7$) leads to a strong reduction of the band gap to 0.04 eV. From the atom-decomposed DOS spectra in Fig. 9, one can see that the Ge atom only, is the origin of the flat energy branches at the vicinity of the Fermi level, which mainly regulates the semiconductor phase of the lateral heterostructures. To obtain more insight into the band gap origin, the PDOS spectra of interline Ge atoms are calculated, the results are given in Fig. 10. One can see that both the upper part of the valence band and the lower part of the conduction band are formed mainly by the p_z state. Such that the band gap

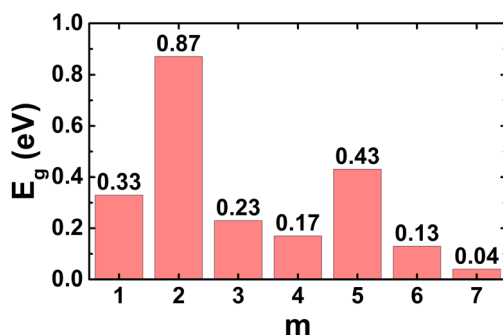


Fig. 8 Electronic band gap of armchair-interline $(Ge)_m-(AsSb)_{8-m}$ lateral heterostructures.

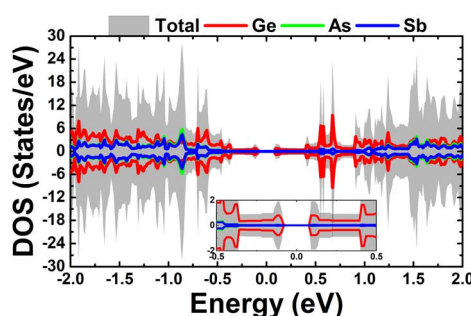


Fig. 9 Total and atom-decomposed density of states of the armchair-interline $(Ge)_4-(AsSb)_4$ lateral heterostructure.

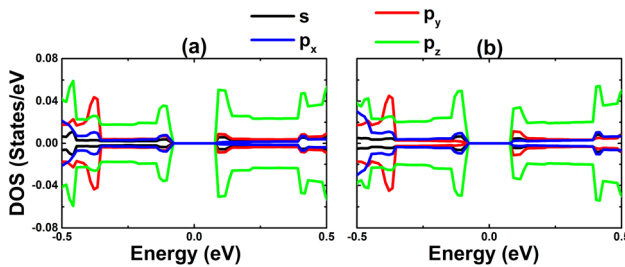


Fig. 10 Projected density of states of interline Ge atoms of armchair-interline $(Ge)_4-(AsSb)_4$ lateral heterostructure: Ge atom of (a) Ge-As and (b) Ge-Sb chemical bonds.

appears due to the separation of Ge- p_z and its value may be impacted by the charge redistribution in this electronic state, which depends on the width of germanene layers. Therefore, it can be concluded that the germanene monolayer band gap can be significantly increased by in-plane interfacial engineering with semiconductor monolayers.

C. Zigzag-interline lateral heterostructures

Similar to the previous cases of armchair-interline LHSs, the atomic structures of the zigzag structures are optimized before proceeding with the calculation of electronic and magnetic properties. The variation of unit cell dimensions as a function of chemical composition (number of germanene units) is illustrated in Fig. 11. As expected, the lattice constants increase in order to incorporate more germanene blocks into the lateral heterostructures to satisfy the size criterion, exhibiting a nearly linear relation.

Fig. 12 shows the calculated band structures of $Z-(Ge)_{m-}(AsSb)_{8-m}$ LHSs considering the energy range -2 to 2 eV, where all exhibit clear spin polarization except for $m = 1$ (Fig. 12a). In all cases, the multivalley in both the valence band and conduction band, induces the quantum valley Hall effect. The valence band and conduction band are connected by flat energy branches, leading to the appearance of topological phases. Normally, the topological phases are obtained in nanoribbons, where the edge states connect the valence band and conduction band.^{73,74} Therefore, our results may introduce a new efficient approach to obtain a topological phase in 2D materials, with both gap and gapless topological interface states. Moreover, new $(Ge)_m-(AsSb)_{8-m}$ LHSs can be considered as potential materials for spintronic applications with quantum spin-valley Hall effects. To analyze the band structure formation, the atom-decomposed DOS spectra are given in Fig. 13. Note that the flat states around the Fermi level are formed mainly from Ge atoms. Therefore, one can conclude that the interface states originate mainly from Ge atoms at the interfaces. Interestingly,

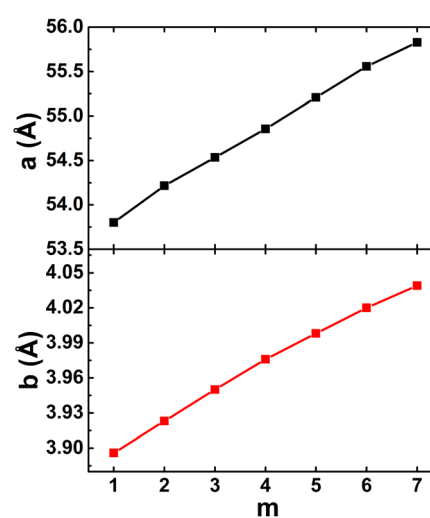


Fig. 11 Lattice constants of zigzag-interline $(Ge)_m-(AsSb)_{8-m}$ lateral heterostructures.



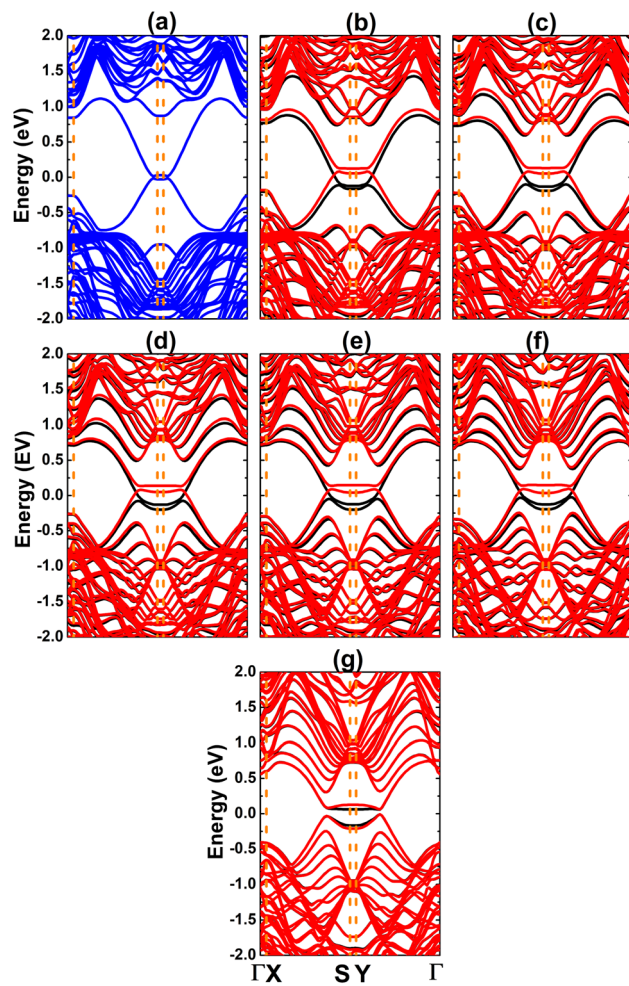


Fig. 12 Electronic band structure (blue curve: non-spin-polarization; black curve: spin-up; red curve: spin-down) of zigzag-interline $(\text{Ge})_m-(\text{AsSb})_{8-m}$ lateral heterostructures with (a) $m = 1$, (b) $m = 2$, (c) $m = 3$, (d) $m = 4$, (e) $m = 5$, (f) $m = 6$, and (g) $m = 7$.

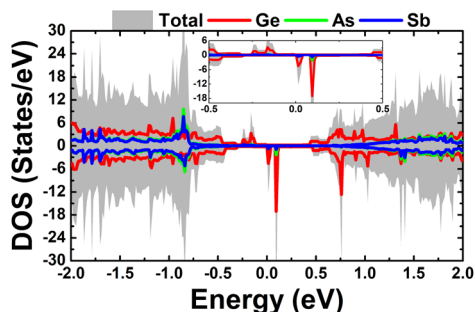


Fig. 13 Total and atom-decomposed density of states of zigzag-interline $(\text{Ge})_4-(\text{AsSb})_4$ lateral heterostructure.

the interface states show Weyl semimetal character with the presence of Fermi-arc states⁷⁵ (see Fig. S3 of the ESI† for band structures from -0.5 to 0.5 eV) enriching the ground state properties of the studied lateral heterostructures, making them promising candidates for practical applications.

Interestingly, our simulations show the emergence of magnetism in zigzag-interline $(\text{Ge})_m-(\text{AsSb})_{8-m}$ LHSs depending on their chemical composition. This feature is reflected in the total magnetic moments, which are given in Fig. 14. Note that the non-magnetic nature of separated monolayers is preserved when forming the $(\text{Ge})_1-(\text{AsSb})_7$ LHS. The magnetization takes place with germanene composition between 25% ($m = 2$) and 75% ($m = 6$) with magnetic moments between $0.46 \mu_B$ and $0.49 \mu_B$. Meanwhile, a small value of only $0.01 \mu_B$ is obtained for the $(\text{Ge})_7-(\text{AsSb})_1$ LHS, suggesting its low magnetization. The origin of magnetism is examined through the spin density illustrated in Fig. 15. From the figure, one can see that the magnetic properties are produced mainly at interfaces. Herein, the spin-up state of Ge atoms plays a key role in the origin of magnetism, meanwhile As and Sb atoms exhibit a small contribution. All these features agree well with the band structure profiles, where the spin polarization ($m = 2$ to 7) is observed only for edge states. The PDOS spectra of Ge, As, and Sb atoms at the interlines of $(\text{Ge})_4-(\text{AsSb})_4$ LHS are displayed in Fig. 16, as an example, to provide more insight. The degree of spin asymmetry can be attributed to the LHS magnetization of the Ge-p_z state. However, we should not neglect the role of the Ge-s, As(Sb)-p_x, and As(Sb)-p_z states considering their presence at the vicinity of the Fermi level, which generate the edge states along with the Ge-p_z state.

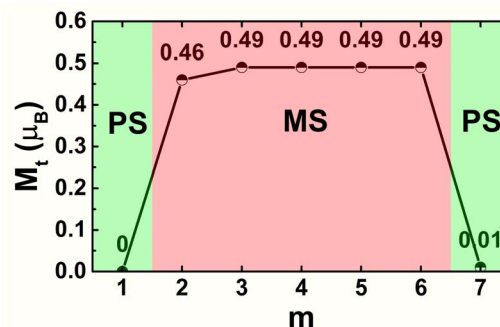


Fig. 14 Total magnetic moment M_t of zigzag-interline $(\text{Ge})_m-(\text{AsSb})_{8-m}$ lateral heterostructures (PS: paramagnetic state; MS: magnetic state).

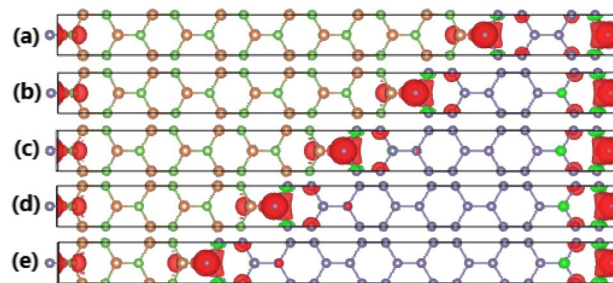


Fig. 15 Spin density (red surface: spin-up state; green surface: spin-down state; iso-surface value: $0.0005 \text{ e } \text{\AA}^{-3}$) in $(\text{Ge})_m-(\text{AsSb})_{8-m}$ lateral heterostructures with (a) $m = 2$, (b) $m = 3$, (c) $m = 4$, (d) $m = 5$, and (e) $m = 6$.

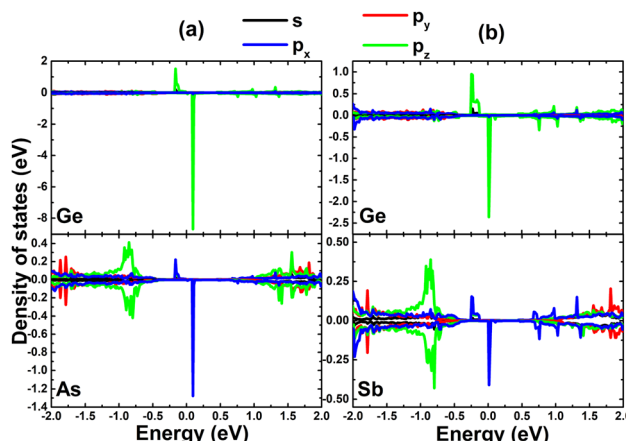


Fig. 16 Projected density of states of the interline atoms of the zigzag interline $(\text{Ge})_4-(\text{AsSb})_4$ lateral heterostructure: (a) Ge–As and (b) Ge–Sb chemical bonds.

IV. Conclusions

In summary, first-principles calculations have been performed to investigate the structural, electronic, and magnetic properties of germanene and AsSb monolayers, as well as their lateral heterostructures. Germanene is a 2D semimetal with Dirac cone at the K point. Meanwhile, the AsSb monolayer is proven to be dynamically stable and exhibits semiconductor character with a band gap of 1.47 eV. A small lattice mismatch of 2.53% may favor the formation of lateral heterostructures, where Z-LHSSs are energetically more favorable than A-LHSSs due to their smaller formation energy. Following the size criterion, the unit cell dimensions increase according to increasing germanene composition. The main contribution of Ge atoms at the vicinity of the Fermi level suggest a band gap increase of the germanene monolayer caused by the in-plane interfacial contact with semiconductor AsSb monolayer along the armchair line. Meanwhile, the Z-LHSSs band structure shows rich electronic features with topological phase, where the valence band and conduction band are connected by interface states. The multi-valley profiles of both the valence band and conduction band may suggest the quantum spin-valley Hall effects for different magnetic applications. In these cases, magnetic properties are produced mainly by the spin-up of interface Ge atoms (Ge- p_z state). Our findings may pave a new way to obtain new 2D materials with either semiconductor or topological phases, with the latter rare in 2D materials at equilibrium.

Computational resources

Calculations were performed at the DGCTIC-UNAM Supercomputing Center (projects LANCAD-UNAM-DGTIC-368).

Data availability

The data that support the findings of this study are available from the corresponding author upon request.

Conflicts of interest

The authors declare that they have no known competing financial interests or personal relationships that could have appeared to influence the work reported in this paper.

Acknowledgements

This research is funded by the Vietnam National Foundation for Science and Technology Development (NAFOSTED) under grant number 103.03-2018.358. Pham Quynh Trang would like to extend her gratitude to Thai Nguyen University of Education for their support.

References

- 1 K. S. Novoselov, A. K. Geim, S. V. Morozov, D.-e. Jiang, Y. Zhang, S. V. Dubonos, I. V. Grigorieva and A. A. Firsov, Electric field effect in atomically thin carbon films, *Science*, 2004, **306**(5696), 666–669.
- 2 M. J. Allen, V. C. Tung and R. B. Kaner, Honeycomb carbon: a review of graphene, *Chem. Rev.*, 2010, **110**(1), 132–145.
- 3 X. J. Lee, B. Y. Z. Hiew, K. C. Lai, L. Y. Lee, S. Gan, S. Thangalazhy-Gopakumar and S. Rigby, Review on graphene and its derivatives: Synthesis methods and potential industrial implementation, *J. Taiwan Inst. Chem. Eng.*, 2019, **98**, 163–180.
- 4 M. Tahriri, M. Del Monico, A. Moghanian, M. T. Yaraki, R. Torres, A. Yadegari and L. Tayebi, Graphene and its derivatives: Opportunities and challenges in dentistry, *Mater. Sci. Eng., C*, 2019, **102**, 171–185.
- 5 K. K. Kim, A. Hsu, X. Jia, S. M. Kim, Y. Shi, M. Hofmann, D. Nezich, J. F. Rodriguez-Nieva, M. Dresselhaus, T. Palacios, *et al.*, Synthesis of monolayer hexagonal boron nitride on Cu foil using chemical vapor deposition, *Nano Lett.*, 2012, **12**(1), 161–166.
- 6 Z. Lin, M. T. Thee, A. L. Elías, S. Feng, C. Zhou, K. Fujisawa, N. Perea-López, V. Carozo, H. Terrones and M. Terrones, Facile synthesis of MoS_2 and $\text{Mo}_{x}\text{W}_{1-x}\text{S}_2$ triangular monolayers, *APL Mater.*, 2014, **2**(9), 092514.
- 7 H. Zhang, M. Holbrook, F. Cheng, H. Nam, M. Liu, C.-R. Pan, D. West, S. Zhang, M.-Y. Chou and C.-K. Shih, Epitaxial growth of two-dimensional insulator monolayer honeycomb BeO , *ACS Nano*, 2021, **15**(2), 2497–2505.
- 8 B. Luo, Y. Yao, E. Tian, H. Song, X. Wang, G. Li, K. Xi, B. Li, H. Song and L. Li, Graphene-like monolayer monoxides and monochlorides, *Proc. Natl. Acad. Sci. U. S. A.*, 2019, **116**(35), 17213–17218.
- 9 H. Şahin, S. Cahangirov, M. Topsakal, E. Bekaroglu, E. Akturk, R. T. Senger and S. Ciraci, Monolayer honeycomb structures of group-IV elements and III-V binary compounds: First-principles calculations, *Phys. Rev. B: Condens. Matter Mater. Phys.*, 2009, **80**(15), 155453.
- 10 H. Zheng, X.-B. Li, N.-K. Chen, S.-Y. Xie, W. Q. Tian, Y. Chen, H. Xia, S. Zhang and H.-B. Sun, Monolayer II-VI semiconductors: A first-principles prediction, *Phys. Rev. B: Condens. Matter Mater. Phys.*, 2015, **92**(11), 115307.



11 A. Gupta, T. Sakthivel and S. Seal, Recent development in 2D materials beyond graphene, *Prog. Mater. Sci.*, 2015, **73**, 44–126.

12 J. R. Schaibley, H. Yu, G. Clark, P. Rivera, J. S. Ross, K. L. Seyler, W. Yao and X. Xu, Valleytronics in 2D materials, *Nat. Rev. Mater.*, 2016, **1**(11), 1–15.

13 B. Luo, G. Liu and L. Wang, Recent advances in 2D materials for photocatalysis, *Nanoscale*, 2016, **8**(13), 6904–6920.

14 J. An, X. Zhao, Y. Zhang, M. Liu, J. Yuan, X. Sun, Z. Zhang, B. Wang, S. Li and D. Li, Perspectives of 2D materials for optoelectronic integration, *Adv. Funct. Mater.*, 2022, **32**(14), 2110119.

15 H. Shu, X. Niu, X. Ding and Y. Wang, Effects of strain and surface modification on stability, electronic and optical properties of GaN monolayer, *Appl. Surf. Sci.*, 2019, **479**, 475–481.

16 T. Kuila, S. Bose, A. K. Mishra, P. Khanra, N. H. Kim and J. H. Lee, Chemical functionalization of graphene and its applications, *Prog. Mater. Sci.*, 2012, **57**(7), 1061–1105.

17 S. Tiwari, M. L. Van de Put, B. Sorée and W. G. Vandenberghe, Magnetic order and critical temperature of substitutionally doped transition metal dichalcogenide monolayers, *npj 2D Mater. Appl.*, 2021, **5**(1), 54.

18 D. Hoat, D. K. Nguyen, J. Guerrero-Sanchez, R. Ponce-Pérez, V. Van On, J. Rivas-Silva and G. H. Cocoletzi, Engineering the electronic and magnetic properties of nitrogen monolayer and bilayer by doping: A first-principles study, *Appl. Surf. Sci.*, 2021, **566**, 150711.

19 G. Zhang and Y.-W. Zhang, Strain effects on thermoelectric properties of two-dimensional materials, *Mech. Mater.*, 2015, **91**, 382–398.

20 G. G. Naumis, S. Barraza-Lopez, M. Oliva-Leyva and H. Terrones, Electronic and optical properties of strained graphene and other strained 2D materials: a review, *Rep. Prog. Phys.*, 2017, **80**(9), 096501.

21 D. Hoat, M. Naseri, R. Ponce-Pérez, N. N. Hieu, T. V. Vu, J. Rivas-Silva and G. H. Cocoletzi, Reducing the electronic band gap of BN monolayer by coexistence of P(As)-doping and external electric field, *Superlattices Microstruct.*, 2020, **137**, 106357.

22 K. K. Kim, H. S. Lee and Y. H. Lee, Synthesis of hexagonal boron nitride heterostructures for 2D van der Waals electronics, *Chem. Soc. Rev.*, 2018, **47**(16), 6342–6369.

23 A. Azizi, S. Eichfeld, G. Geschwind, K. Zhang, B. Jiang, D. Mukherjee, L. Hossain, A. F. Piasecki, B. Kabius, J. A. Robinson, *et al.*, Freestanding van der waals heterostructures of graphene and transition metal dichalcogenides, *ACS Nano*, 2015, **9**(5), 4882–4890.

24 F. Li, B. Xu, W. Yang, Z. Qi, C. Ma, Y. Wang, X. Zhang, Z. Luo, D. Liang, D. Li, *et al.*, High-performance optoelectronic devices based on van der Waals vertical MoS₂/MoSe₂ heterostructures, *Nano Res.*, 2020, **13**, 1053–1059.

25 F. Ceballos, M. Z. Bellus, H.-Y. Chiu and H. Zhao, Ultrafast charge separation and indirect exciton formation in a MoS₂–MoSe₂ van der Waals heterostructure, *ACS Nano*, 2014, **8**(12), 12717–12724.

26 W. Liao, Y. Huang, H. Wang and H. Zhang, Van der Waals heterostructures for optoelectronics: progress and prospects, *Appl. Mater. Today*, 2019, **16**, 435–455.

27 Y. Liu, N. O. Weiss, X. Duan, H.-C. Cheng, Y. Huang and X. Duan, Van der Waals heterostructures and devices, *Nat. Rev. Mater.*, 2016, **1**(9), 1–17.

28 X.-Q. Zhang, C.-H. Lin, Y.-W. Tseng, K.-H. Huang and Y.-H. Lee, Synthesis of lateral heterostructures of semiconducting atomic layers, *Nano Lett.*, 2015, **15**(1), 410–415.

29 J. Zhao, K. Cheng, N. Han and J. Zhang, Growth control, interface behavior, band alignment, and potential device applications of 2D lateral heterostructures, *Wiley Interdiscip. Rev.: Comput. Mol. Sci.*, 2018, **8**(2), e1353.

30 J. Lee, S. Pak, Y.-W. Lee, Y. Park, A.-R. Jang, J. Hong, Y. Cho, B. Hou, S. Lee, H. Y. Jeong, *et al.*, Direct epitaxial synthesis of selective two-dimensional lateral heterostructures, *ACS Nano*, 2019, **13**(11), 13047–13055.

31 M. P. Levendorf, C.-J. Kim, L. Brown, P. Y. Huang, R. W. Havener, D. A. Muller and J. Park, Graphene and boron nitride lateral heterostructures for atomically thin circuitry, *Nature*, 2012, **488**(7413), 627–632.

32 J. Wang, Z. Li, H. Chen, G. Deng and X. Niu, Recent advances in 2D lateral heterostructures, *Nano-Micro Lett.*, 2019, **11**, 1–31.

33 M. E. Dávila and G. Le Lay, Few layer epitaxial germanene: a novel two-dimensional dirac material, *Sci. Rep.*, 2016, **6**(1), 1–9.

34 Z. Qin, J. Pan, S. Lu, Y. Shao, Y. Wang, S. Du, H.-J. Gao and G. Cao, Direct evidence of Dirac signature in bilayer germanene islands on Cu (111), *Adv. Mater.*, 2017, **29**(13), 1606046.

35 L. Kesper, J. A. Hochhaus, M. Schmitz, M. G. Schulte, U. Berges and C. Westphal, Tracing the structural evolution of quasi-freestanding germanene on Ag (111), *Sci. Rep.*, 2022, **12**(1), 7559.

36 L. Li, S.-z. Lu, J. Pan, Z. Qin, Y.-q. Wang, Y. Wang, G.-y. Cao, S. Du and H.-J. Gao, Buckled germanene formation on Pt (111), *Adv. Mater.*, 2014, **26**(28), 4820–4824.

37 M. Derivaz, D. Dentel, R. Stephan, M.-C. Hanf, A. Mehdaoui, P. Sonnet and C. Pirri, Continuous germanene layer on Al (111), *Nano Lett.*, 2015, **15**(4), 2510–2516.

38 L. Zhang, P. Bampoulis, A. Rudenko, Q. v. Yao, A. Van Houselt, B. Poelsema, M. Katsnelson and H. Zandvliet, Structural and electronic properties of germanene on MoS₂, *Phys. Rev. Lett.*, 2016, **116**(25), 256804.

39 X.-S. Ye, Z.-G. Shao, H. Zhao, L. Yang and C.-L. Wang, Intrinsic carrier mobility of germanene is larger than graphene's: first-principle calculations, *RSC Adv.*, 2014, **4**(41), 21216–21220.

40 M. Ezawa, Monolayer topological insulators: silicene, germanene, and stanene, *J. Phys. Soc. Jpn.*, 2015, **84**(12), 121003.

41 M. Ye, R. Quhe, J. Zheng, Z. Ni, Y. Wang, Y. Yuan, G. Tse, J. Shi, Z. Gao and J. Lu, Tunable band gap in germanene by surface adsorption, *Phys. E*, 2014, **59**, 60–65.



42 D. Hoat, D. K. Nguyen, R. Ponce-Perez, J. Guerrero-Sanchez, V. Van On, J. Rivas-Silva and G. H. Cocoletzi, Opening the germanene monolayer band gap using halogen atoms: An efficient approach studied by first-principles calculations, *Appl. Surf. Sci.*, 2021, **551**, 149318.

43 M. Köpf, N. Eckstein, D. Pfister, C. Grotz, I. Krüger, M. Greiwe, T. Hansen, H. Kohlmann and T. Nilges, Access and in situ growth of phosphorene-precursor black phosphorus, *J. Cryst. Growth*, 2014, **405**, 6–10.

44 W. Zhang, H. Enriquez, Y. Tong, A. Bendounan, A. Kara, A. P. Seitsonen, A. J. Mayne, G. Dujardin and H. Oughaddou, Epitaxial synthesis of blue phosphorene, *Small*, 2018, **14**(51), 1804066.

45 J.-S. Li, W.-L. Wang and D.-X. Yao, Band gap engineering of two-dimensional nitrogen, *Sci. Rep.*, 2016, **6**(1), 34177.

46 W. Lin, J. Li, W. Wang, S.-D. Liang and D.-X. Yao, Electronic structure and band gap engineering of two-dimensional octagon-nitrogen, *Sci. Rep.*, 2018, **8**(1), 1674.

47 A. Carvalho, M. Wang, X. Zhu, A. S. Rodin, H. Su and A. H. Castro Neto, Phosphorene: from theory to applications, *Nat. Rev. Mater.*, 2016, **1**(11), 1–16.

48 A. H. Woerner, T. W. Farnsworth, J. Hu, R. A. Wells, C. L. Donley and S. C. Warren, Phosphorene: synthesis, scale-up, and quantitative optical spectroscopy, *ACS Nano*, 2015, **9**(9), 8869–8884.

49 J. Shah, W. Wang, H. M. Sohail and R. Uhrberg, Experimental evidence of monolayer arsenene: an exotic 2D semiconducting material, *2D Mater.*, 2020, **7**(2), 025013.

50 P. Jamdagni, A. Thakur, A. Kumar, P. Ahluwalia and R. Pandey, Two dimensional allotropes of arsenene with a wide range of high and anisotropic carrier mobility, *Phys. Chem. Chem. Phys.*, 2018, **20**(47), 29939–29950.

51 Y. Shao, Z.-L. Liu, C. Cheng, X. Wu, H. Liu, C. Liu, J.-O. Wang, S.-Y. Zhu, Y.-Q. Wang, D.-X. Shi, *et al.*, Epitaxial growth of flat antimonene monolayer: A new honeycomb analogue of graphene, *Nano Lett.*, 2018, **18**(3), 2133–2139.

52 D. Singh, S. K. Gupta, Y. Sonvane and I. Lukačević, Antimonene: a monolayer material for ultraviolet optical nanodevices, *J. Mater. Chem. C*, 2016, **4**(26), 6386–6390.

53 J. Zhou, J. Chen, M. Chen, J. Wang, X. Liu, B. Wei, Z. Wang, J. Li, L. Gu, Q. Zhang, *et al.*, Few-layer bismuthene with anisotropic expansion for high-areal-capacity sodium-ion batteries, *Adv. Mater.*, 2019, **31**(12), 1807874.

54 R.-B. Chen, D.-J. Jang, M.-C. Lin and M.-F. Lin, Optical properties of monolayer bismuthene in electric fields, *Opt. Lett.*, 2018, **43**(24), 6089–6092.

55 M. Long, A. Gao, P. Wang, H. Xia, C. Ott, C. Pan, Y. Fu, E. Liu, X. Chen, W. Lu, *et al.*, Room temperature high-detectivity mid-infrared photodetectors based on black arsenic phosphorus, *Sci. Adv.*, 2017, **3**(6), e1700589.

56 W. Yu, C.-Y. Niu, Z. Zhu, X. Cai, L. Zhang, S. Bai, R. Zhao and Y. Jia, Strain induced quantum spin hall insulator in monolayer β -BiSb from first-principles study, *RSC Adv.*, 2017, **7**(44), 27816–27822.

57 X.-Y. Lin, F.-S. Meng, Q.-C. Liu, Q. Xue and H. Zhang, Semiconducting two-dimensional group VA-VA haeckelite compounds with superior carrier mobility, *Phys. Chem. Chem. Phys.*, 2020, **22**(21), 12260–12266.

58 W. Yu, C.-Y. Niu, Z. Zhu, X. Wang and W.-B. Zhang, Atomically thin binary V-V compound semiconductor: a first-principles study, *J. Mater. Chem. C*, 2016, **4**(27), 6581–6587.

59 W. Kohn and L. J. Sham, Self-consistent equations including exchange and correlation effects, *Phys. Rev.*, 1965, **140**(4A), A1133.

60 G. Kresse and J. Furthmüller, Efficiency of ab-initio total energy calculations for metals and semiconductors using a plane-wave basis set, *Comput. Mater. Sci.*, 1996, **6**(1), 15–50.

61 G. Kresse and J. Furthmüller, Efficient iterative schemes for ab initio total-energy calculations using a plane-wave basis set, *Phys. Rev. B: Condens. Matter*, 1996, **54**(16), 11169.

62 J. P. Perdew, K. Burke and M. Ernzerhof, Generalized gradient approximation made simple, *Phys. Rev. Lett.*, 1996, **77**(18), 3865.

63 J. Heyd, G. E. Scuseria and M. Ernzerhof, Hybrid functionals based on a screened Coulomb potential, *J. Chem. Phys.*, 2003, **118**(18), 8207–8215.

64 A. V. Krukau, O. A. Vydrov, A. F. Izmaylov and G. E. Scuseria, Influence of the exchange screening parameter on the performance of screened hybrid functionals, *J. Chem. Phys.*, 2006, **125**(22), 224106.

65 H. J. Monkhorst and J. D. Pack, Special points for Brillouin-zone integrations, *Phys. Rev. B: Solid State*, 1976, **13**(12), 5188.

66 M. Sun, Q. Ren, S. Wang, Y. Zhang, Y. Du, J. Yu and W. Tang, Magnetism in transition-metal-doped germanene: a first-principles study, *Comput. Mater. Sci.*, 2016, **118**, 112–116.

67 L. Pardini, S. Löffler, G. Biddau, R. Hambach, U. Kaiser, C. Draxl and P. Schattschneider, Mapping atomic orbitals with the transmission electron microscope: Images of defective graphene predicted from first-principles theory, *Phys. Rev. Lett.*, 2016, **117**(3), 036801.

68 F. Ersan, E. Aktürk and S. Ciraci, Stable single-layer structure of group-V elements, *Phys. Rev. B*, 2016, **94**(24), 245417.

69 G.-X. Chen, X.-G. Li, Y.-P. Wang, J. N. Fry and H.-P. Cheng, Two-dimensional lateral GaN/SiC heterostructures: First-principles studies of electronic and magnetic properties, *Phys. Rev. B*, 2017, **95**(4), 045302.

70 G. H. Han, J. A. Rodríguez-Manzo, C.-W. Lee, N. J. Kybert, M. B. Lerner, Z. J. Qi, E. N. Dattoli, A. M. Rappe, M. Drndic and A. C. Johnson, Continuous growth of hexagonal graphene and boron nitride in-plane heterostructures by atmospheric pressure chemical vapor deposition, *ACS Nano*, 2013, **7**(11), 10129–10138.

71 T. Ogikubo, H. Shimazu, Y. Fujii, K. Ito, A. Ohta, M. Araida, M. Kurosawa, G. Le Lay and J. Yuhara, Continuous growth of germanene and stanene lateral heterostructures, *Adv. Mater. Interfaces*, 2020, **7**(10), 1902132.

72 B. Kundu, P. Mohanty, P. Kumar, B. Nayak, B. Mahato, P. Ranjan, S. K. Chakraborty, S. Sahoo and P. K. Sahoo, Synthesis of lateral heterostructure of 2D materials for optoelectronic devices: challenges and opportunities, *Emergent Mater.*, 2021, **4**(4), 923–949.



73 B. Fu, M. Abid and C.-C. Liu, Systematic study on stanene bulk states and the edge states of its zigzag nanoribbon, *New J. Phys.*, 2017, **19**(10), 103040.

74 K. W. Lee and C. E. Lee, Quantum valley Hall effect in wide-gap semiconductor SiC monolayer, *Sci. Rep.*, 2020, **10**(1), 5044.

75 X. Wan, A. M. Turner, A. Vishwanath and S. Y. Savrasov, Topological semimetal and Fermi-arc surface states in the electronic structure of pyrochlore iridates, *Phys. Rev. B: Condens. Matter Mater. Phys.*, 2011, **83**(20), 205101.

